Available online at www.sciencedirect.com
SCIENCE DIRECT®
International Journal of Heat and Mass Transfer 49 (2006) 1162–1175
International Journal of HEAT and MASS TRANSFER
www.elsevier.com/locate/ijhmt

Direct numerical simulation of wall-normal rotating turbulent channel flow with heat transfer

Bu-Yang Li, Nan-Sheng Liu, Xi-Yun Lu *

Department of Modern Mechanics, University of Science and Technology of China, Hefei, Anhui 230026, PR China

Received 6 April 2005; received in revised form 25 July 2005
Available online 18 October 2005

Abstract

Direct numerical simulation of wall-normal rotating channel flow with heat transfer has been performed for the rotation number N_τ from 0 to 0.1, the Reynolds number 194 based on the friction velocity of non-rotating case and the half-height of the channel, and the Prandtl number 1. The objective of this study is to reveal the effects of rotation on the characteristics of turbulence and heat transfer. Some statistical turbulence and heat transfer quantities, including the mean velocity, temperature and their fluctuations, turbulent heat fluxes, and turbulence structures, are investigated. Based on the present calculated results, two typical rotation regimes are identified. When $0 < N_\tau < 0.06$, the turbulence statistics correlated with the spanwise velocity fluctuation are enhanced since the shear rate of spanwise mean flow induced by Coriolis force increases; however, the other statistics are suppressed. When $N_\tau > 0.06$, all the turbulence statistics are suppressed significantly. To elucidate the effects of rotation on the turbulent heat transfer, the budget terms in the transport equation of turbulent heat fluxes are analyzed. Remarkable change of the direction of near-wall streak structures of the velocity and temperature fluctuations, nearly in alignment with the absolute mean flow direction, is revealed. An attempt to evaluate the mean spacing and the direction of streaky structures near the wall has been examined based on the two-point correlations of the velocity and temperature fluctuations.

Keywords: Direct numerical simulation (DNS); Wall-normal rotating channel flow; Turbulent heat transfer; Thermal statistics; Coherent structure

1. Introduction

Turbulent flows with heat transfer in rotating frame exist in a variety of industrial, geophysical and astrophysical applications. The rotation induces additional body forces, i.e., centrifugal and Coriolis forces, acting on the turbulent flow, so that the momentum transfer mechanism becomes more complex. Understanding the mechanism is of great importance in applications and fundamentals and is highly desired. Usually, a simple and convenient way to investigate rotating turbulent flow is rotating channel flows, where the rotating axis can be chosen as that parallel to one of the three directions, i.e., the streamwise, spanwise and wall-normal directions [1].

As well known, the spanwise rotating turbulent channel flows have been extensively studied experimentally and numerically [2–7]. With increasing the rotation rate, turbulence is gradually enhanced on the pressure side and reduced on the suction side. Meanwhile, large-scale rotational-induced roll cells due to Taylor–Görtler instability occur in the cross-sectional plane of the channel and shift towards the pressure side wall [2,3]. On the other hand, some work has also been undertaken to study the streamwise rotating turbulent channel flows. Comparing with the spanwise rotation effect, the influence of streamwise rotation on turbulent channel flow is much weak [1,8]. The streamwise rotation induces a mean velocity in the spanwise direction. The quasi-streamwise near-wall vortical structures rotating in the same direction are enhanced, whereas the opposite ones are reduced, and consequently the average spacing between the low- and

* Corresponding author. Tel.: +86 551 3603223; fax: +86 551 3606459.
E-mail address: xlu@ustc.edu.cn (X.-Y. Lu).

0017-9310/$ - see front matter © 2005 Elsevier Ltd. All rights reserved.
doi:10.1016/j.ijheatmasstransfer.2005.08.030

Nomenclature

B_T	additive constant in the logarithmic law of the temperature profile
B_u	additive constant in the logarithmic law of the streamwise velocity profile
B_w	additive constant in the logarithmic law of the spanwise velocity profile
h	half-height of the channel
k	thermal conductivity
K_T	von Kárman constant in the logarithmic law of the temperature profile
K_u	von Kárman constant in the logarithmic law of the streamwise velocity profile
K_w	von Kárman constant in the logarithmic law of the spanwise velocity profile
Nu	Nusselt number
N_τ	rotation number
p	effective pressure
Pr	Prandtl number
q_w	mean heat flux at the wall
Re_τ	Reynolds number based on the friction velocity
t	time
T	temperature
T_L	temperature at the lower wall
T_U	temperature at the upper wall
T_τ	friction temperature
T'	temperature fluctuation
u	streamwise velocity
u'	streamwise velocity fluctuation
u_i	velocity component in the i-direction
u_i'	velocity fluctuation in the i-direction
u_τ	friction velocity
v	wall-normal velocity
v'	wall-normal velocity fluctuation
w	spanwise velocity
w'	spanwise velocity fluctuation
x	streamwise coordinate
x_i	Cartesian coordinate axes
y	wall-normal coordinate
y_d	wall-normal distance from the wall
y^+	wall-normal distance from the wall normalized by the friction velocity
z	spanwise coordinate
ν	molecular kinematic viscosity
λ^+	mean spacing between the streaky structures
λ_x^+	mean spacing of the streaky structures along the streamwise direction
λ_z^+	mean spacing of the streaky structures along the spanwise direction
θ_λ	mean inclined angle of the streaky structures
κ	thermal diffusivity
ρ	fluid density
Ω	angular velocity of system rotation
$\langle\rangle$	average in time and in the plane parallel to the wall

Subscript

rms	root mean square

Superscript

$+$	normalized quantity by wall parameters

high-speed streaky structures becomes much larger than that in a non-rotating channel.

In a wall-normal rotating channel flow, since the mean vorticity component is perpendicular to the rotating axis, turbulent channel flow is so sensitive to the wall-normal rotation, even though a slight system rotation can induce a significant spanwise mean velocity [1]. As a result, the absolute mean flow deviates from the initial streamwise direction, which makes all the six components of the Reynolds stress tensor non-zero, and redirects the mean shear and the turbulence structures. The interaction between the vorticity of coherent structures and the background vorticity due to imposed wall-normal rotation can significantly change the near-wall turbulence behavior, and the statistical coherent structures are verified to be more sensitive to the Coriolis force effect induced by the wall-normal rotation [9].

It is well established that direct numerical simulation (DNS) is effective to explore the mechanism of turbulence and heat transfer and to provide in detail statistical quantities which are essential to construct turbulence models [7,10,11]. The determination of the thermal budget terms in the transport equations of turbulent heat fluxes is of great importance to the closure of the turbulent heat fluxes. Based on the DNS of turbulent channel flow with heat transfer, it is found that the temperature–pressure gradient correlation is a dominant term in the budget of wall-normal turbulent heat flux [12,13]. The turbulent diffusion and dissipation terms in the budgets of turbulent heat fluxes are physically meaningful to the construction and assessment of the turbulence model involving heat transfer [7,11]. Thus, it is highly tempting to investigate the effects of rotation on the budget terms of turbulent heat fluxes.

As described above, experimental and numerical investigations on the rotating channel flows mainly focus on the turbulence statistics and near-wall structures without heat transfer [1–6]. Understanding the effects of rotation on turbulent heat transfer in the rotating channel flow is an important fundamental issue in turbulence and thermal modeling because any model aimed at predicting the thermal statistics in rotating turbulence should reproduce the essential features of this canonical situation. To the best of our knowledge, however, little work for the wall-normal rotating channel flow with heat transfer has been

undertaken to elucidate the characteristics of turbulence and heat transfer. In this paper, the effects of rotation on the wall-normal rotating turbulent channel flow with heat transfer are studied by means of DNS.

This paper is organized as follows. The mathematical formulation is described in Section 2. The numerical method is briefly given in Section 3. In Section 4 some statistical turbulence and heat transfer quantities, the budget terms in the transport equations of turbulent heat fluxes, and the near-wall structures are discussed. Finally, concluding remarks are summarized in Section 5.

2. Mathematical formulation

The incompressible Navier–Stokes and energy equations are used for direct simulation of fully developed turbulent flow with a passive heat transfer in a wall-normal rotating channel. To normalize the governing equations, the friction velocity u_τ of non-rotating channel flow is used as the velocity scale, the half-height of the channel h as the length scale, and the temperature difference ΔT between the upper and lower walls as the temperature scale. The non-dimensional governing equations are given as

$$\frac{\partial u_i}{\partial x_i} = 0 \tag{1}$$

$$\frac{\partial u_i}{\partial t} + \frac{\partial u_i u_j}{\partial x_j} = -\frac{\partial p}{\partial x_i} + \delta_{1i} + \frac{1}{Re_\tau}\frac{\partial^2 u_i}{\partial x_j \partial x_j} - N_\tau \varepsilon_{ijk}\frac{\Omega_j}{|\Omega|}u_k \tag{2}$$

$$\frac{\partial T}{\partial t} + \frac{\partial (T u_j)}{\partial x_j} = \frac{1}{Re_\tau Pr}\frac{\partial^2 T}{\partial x_j \partial x_j} \tag{3}$$

where p represents the effective pressure combined with the centrifugal force. The non-dimensional parameters in this problem are the rotation, Reynolds and Prandtl numbers, which are defined as $N_\tau = 2|\Omega|h/u_\tau$, $Re_\tau = u_\tau h/\nu$ and $Pr = \nu/\kappa$, respectively, with Ω being the angular speed of rotating frame, ν the kinematic viscosity, and κ the thermal diffusivity.

As shown in Fig. 1 for the sketch of the wall-normal rotating channel, the flow and temperature fields are assumed to be statistically homogeneous in the streamwise and spanwise directions. Thus, periodic boundary conditions are employed in both the directions. No-slip condition is used on the channel walls. Two different constant temperatures, i.e., $T_U = 0.5$ and $T_L = -0.5$, are imposed on the upper and lower walls, respectively. Heat transfer computation is started after the flow field has statistically reached a fully developed turbulent state. Initial temperature field is set to be a linear distribution along the wall-normal direction and homogeneous in the plane parallel to the wall.

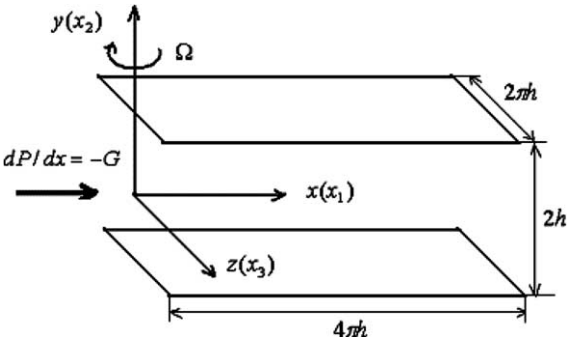

Fig. 1. Sketch of the wall-normal rotating channel flow with heat transfer.

3. Numerical methods

To solve Eqs. (1)–(3), a fractional-step method developed by Verzicco and Orlandi [14] is used. Spatial derivatives are discretized by a second-order central difference. Time advancement is carried out by the semi-implicit scheme using the Crank–Nicholson scheme for the viscous terms and the three-stage Runge–Kutta scheme for the convective terms. The discretized formulation was described in detail by Verzicco and Orlandi [14]. This method simplifies the boundary condition of the non-solenoidal velocity field, while remains the feature of the algorithm developed by Kim and Moin [15] and Rai and Moin [16], and has the additional advantage that the minimum amount of computer run-time memory is realized.

In this study, the rotation number is $N_\tau = 0$–0.1, the Reynolds number $Re_\tau = 194$, and the Prandtl number $Pr = 1$. The mesh number is $193 \times 161 \times 129$ corresponding to the computational domain $4\pi h \times 2h \times 2\pi h$ in the streamwise, wall-normal and spanwise directions, respectively. The grid system is enough to resolve all essential scales of the low-Reynolds number turbulence and contains the largest scale structures in the channel [17]. A stretching transformation is employed to obtain fine grid resolution in the wall regions. The grid point close to the wall is located at $y^+ = 0.3$ approximately, while the largest spacing is about $\Delta y^+ = 4.5$ at the center of the channel, where y^+ is defined as $y^+ = (1 - |y/h|)Re_\tau$. Uniform grids are employed in the streamwise and spanwise directions with the grid spacing $\Delta x^+ = 12.6$ and $\Delta z^+ = 9.5$. To ensure the computational domain size to be enough, the two-point correlations of the velocity and temperature fluctuations in the streamwise and spanwise directions shown in following section are calculated to be negligibly small, indicating that the computational domain used is large enough.

It is worthwhile to mention that the performance and reliability of the numerical method employed in this study have been verified extensively based on the DNS of rotating and non-rotating turbulent pipe flows [18–20]. These studies revealed that the second- and higher-order turbulence statistics compared well with available DNS results calculated by the spectral methods and with experimental data. In addition, the finite difference schemes with the second-order accuracy are widely used in the DNS of turbulent and transitional flows, e.g., rotating channel flow [3,21], annular pipe flow [22], oscillatory flow in the boundary layer and pipe [23,24], and turbulent Rayleigh–Bénard convection flow [25]. Thus, it has been confirmed that the

numerical approach with the second-order accuracy schemes can succeed in predicting turbulence characteristics. In the present study, the relevant code and method used were also verified in our previous work [26–33]. In particular, detailed validations including the skewness and flatness of the velocity fluctuations were carried out based on the DNS of stably and unstably stratified open channel flows [33].

4. Results and discussion

4.1. Turbulence statistics

The profiles of the mean velocity in the streamwise and spanwise directions are shown in Fig. 2a and b. As the wall-normal rotation is imposed, the streamwise mean velocity $\langle u \rangle$ decreases monotonically with the increase of N_τ, indicating the reduction of the wall shear rate related to the streamwise mean flow. In Fig. 2b, the spanwise mean velocity $\langle w \rangle$ increases when N_τ varies from 0 to 0.06; however, when N_τ increases further, e.g., at $N_\tau = 0.08$ and 0.1, the spanwise mean flow is suppressed obviously.

Further, by examining the velocity profiles in Fig. 2a and b, a logarithmic form is identified

$$\langle u^+ \rangle = (1/K_u) \ln y^+ + B_u \tag{4a}$$

$$\langle w^+ \rangle = (1/K_w) \ln y^+ + B_w \tag{4b}$$

where K_u and K_w as well as B_u and B_w represent the von Kárman constant and the additive constant in the log law of the velocity profiles, respectively. As shown in Fig. 2c and d, $1/K_u$ and B_u decrease with increasing N_τ; however, $1/K_w$ and B_w vary complexly versus N_τ. As an analogy between the influences of rotation and thermal stratification on turbulent flow [34], the characteristics of the mean velocity are consistent with those in thermally stratified turbulent channel flow [31].

Distributions of the turbulence intensities are shown in Fig. 3, where y_d denotes the distance from the wall, i.e., $y_d = 1 - |y/h|$. In pure shear channel flow, only the streamwise mean velocity exists. The streamwise velocity fluctuation is mainly generated by the shear process of the streamwise mean flow, while the mechanism to generate the spanwise velocity fluctuation is the splattering effect induced by the high-speed streaky structures rushing to the

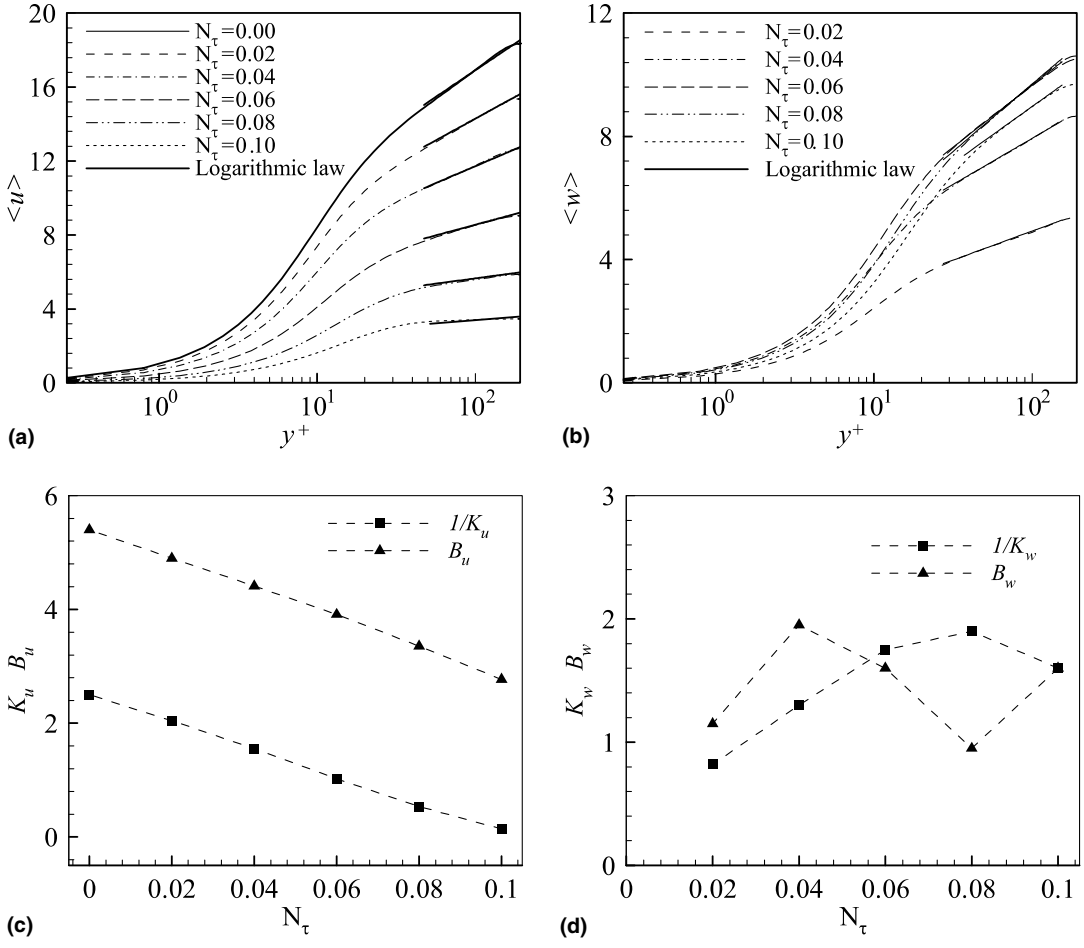

Fig. 2. Profiles of the mean streamwise (a) and spanwise (b) velocity, and the von Kárman constants and the additive constants in the log law of the streamwise (c) and spanwise (d) velocity profiles.

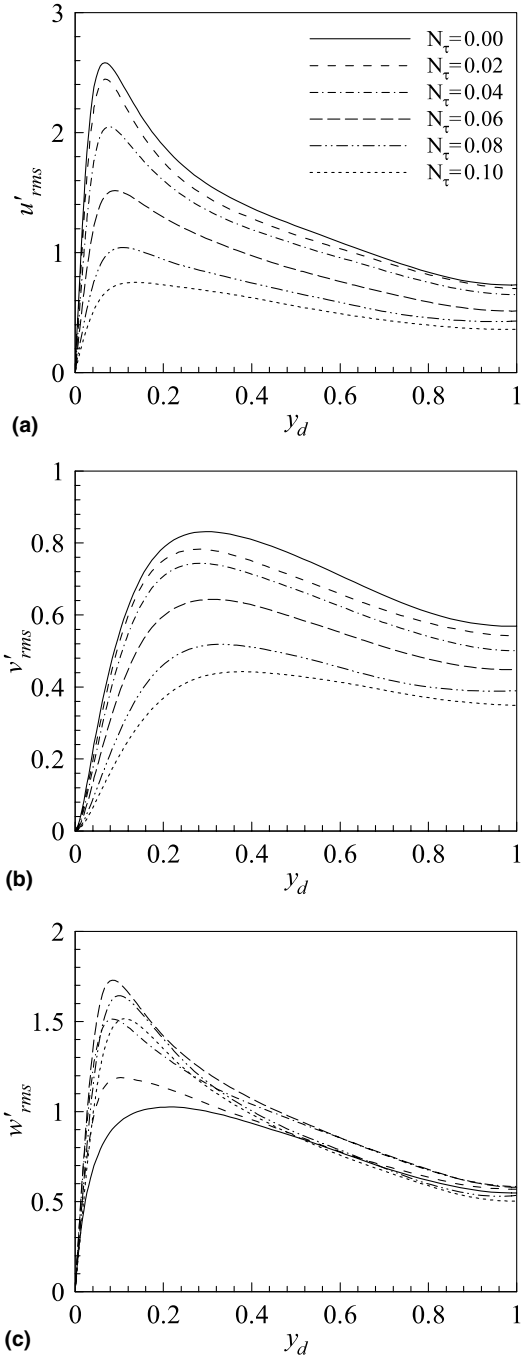

Fig. 3. Turbulence intensities in the streamwise (a), wall-normal (b), and spanwise (c) direction.

wall and the low-speed ones lifting from the wall [35]. However, in the wall-normal rotating channel flow, since the Coriolis force induces the spanwise mean velocity shown in Fig. 2b, there exist both the streamwise and spanwise mean shear effects. Thus, the production of the streamwise velocity fluctuation comes from both processes. One is the shear process related to $\langle u\rangle$, which is the major source to generate the streamwise velocity fluctuation in weakly rotating case, and the other the splattering effect associated with $\langle w\rangle$. So does the spanwise velocity fluctuation, and the shear process of the spanwise mean flow will take a dominate responsibility to generate the spanwise velocity fluctuation in strong rotation case due to the presence of large spanwise mean velocity. Correspondingly, turbulent heat transfer in the spanwise direction is induced significantly due to the spanwise mean flow and will be discussed in the following.

As shown in Fig. 3a, at low rotation number, e.g., $N_\tau = 0.02$, a slight reduction of $u'_{\rm rms}$ in the wall region, in comparison with that of the non-rotating case, is exhibited. The wall-normal intensity $v'_{\rm rms}$ in Fig. 3b has a similar feature with $u'_{\rm rms}$, and the spanwise intensity $w'_{\rm rms}$ in Fig. 3c increases somewhat. This behavior at low rotation number is well consistent with the previous findings [1]. As N_τ increases, the near-wall shear rate related to $\langle u\rangle$ reduces significantly. Thus, a rapid drop of $u'_{\rm rms}$ is observed in Fig. 3a. When N_τ varies from 0 to 0.06, the spanwise velocity fluctuation $w'_{\rm rms}$ is enhanced remarkably due to increasing the spanwise mean shear rate shown in Fig. 2b. The high near-wall peak value of $w'_{\rm rms}$ at $N_\tau = 0.06$ is attributed to strong shear rate of the spanwise mean flow. When the rotation rate increases further, e.g., $N_\tau = 0.08$ and 0.1, the mechanism for turbulence fluctuation generation is suppressed apparently by the Coriolis force effect, which causes the reduction of all three turbulence intensities.

Effects of the wall-normal rotation on the turbulent flow are obviously to change the absolute mean flow direction, i.e., tilting to the spanwise direction. Thus, the elongated streaky structures near the wall generated by the shear process of the absolute mean flow are expected to deviate from the streamwise to the spanwise direction. This suggests that, near the lower wall, the high-speed (relative to the absolute mean flow) streaks, corresponding to the sweep events [17,36], are related to the fluid with velocity fluctuations $u' > 0$, $w' < 0$ and $v' < 0$, while the low-speed streaks responsible for the ejection events correspond to $u' < 0$, $w' > 0$ and $v' > 0$. Similar prediction can be achieved for the elongated streaks near the upper wall. These relations between the velocity fluctuations are helpful to determine the sign of shear stresses in the wall regions.

Fig. 4 shows the profiles of the shear stresses. The shear stresses $\langle u'v'\rangle$ and $\langle u'w'\rangle$ are found to be negative in the lower wall region, while the shear stress $\langle v'w'\rangle$ to be positive, which is consistent with the above description relevant to the ejection and sweep events. The $\langle u'v'\rangle$ is mainly related to the change of $\langle u\rangle$ and subsequently decreases with the increase of N_τ. At low rotation number (e.g., $N_\tau = 0.02$), a slight alteration of the shear stress occurs. However, at high-rotation number, e.g., $N_\tau = 0.1$, the $\langle u'v'\rangle$ becomes nearly zero over the channel, indicating a poor correlation between the streamwise and wall-normal velocity fluctuations subject to strong rotation. The distributions of $\langle u'v'\rangle$ and $\langle v'w'\rangle$ contain a noticeable linear region in the core region which should be ascribed to the co-existence of the streamwise and spanwise mean flows in the rotating cases. The $\langle v'w'\rangle$, which is related to the change of $\langle w\rangle$, is enhanced as N_τ varies from 0 to 0.06 and suppressed as N_τ from 0.06 to 0.1. The near-wall alterations of $\langle v'w'\rangle$

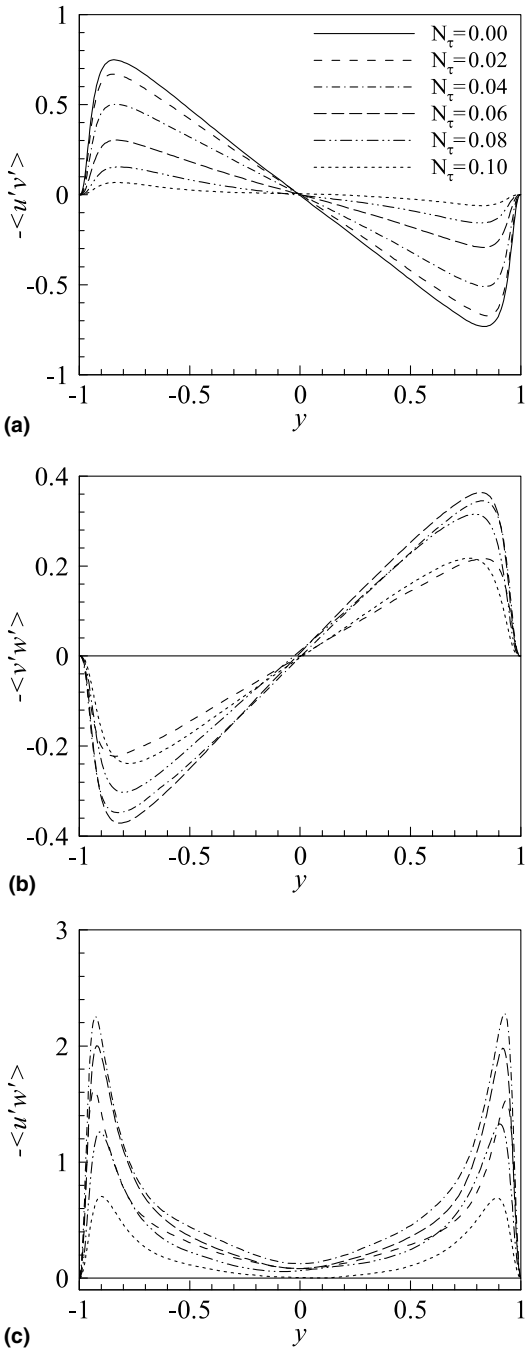

Fig. 4. Profiles of the shear stresses: (a) $\langle u'v' \rangle$, (b) $\langle v'w' \rangle$, and (c) $\langle u'w' \rangle$.

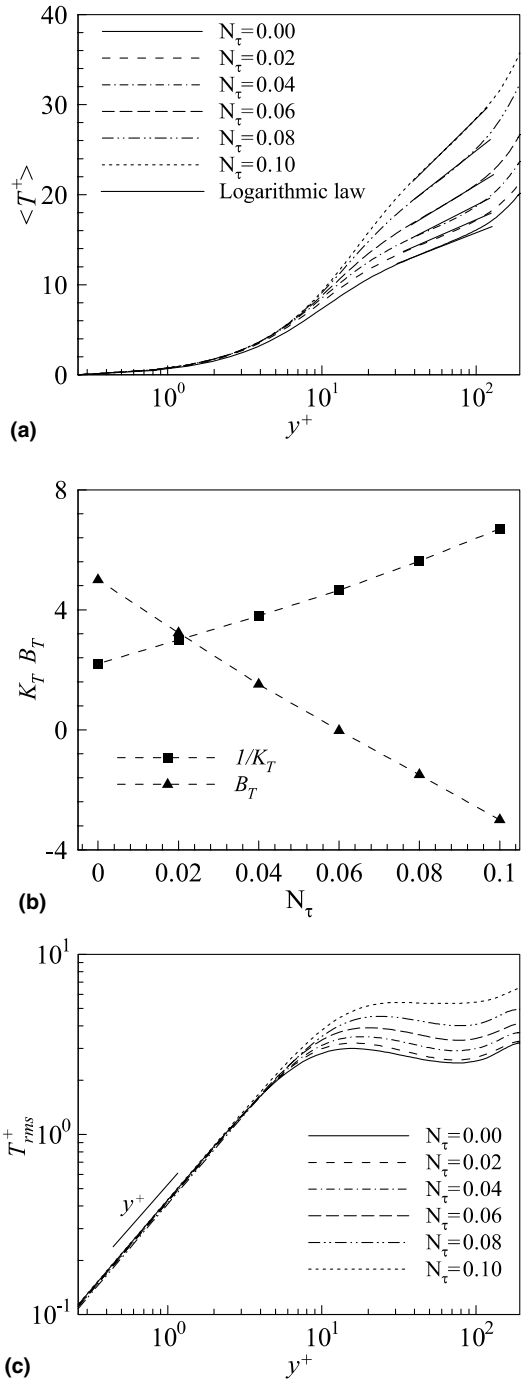

Fig. 5. Temperature statistics: (a) mean temperature, (b) von Kárman constant and additive constant, and (c) temperature fluctuation.

and $\langle u'w' \rangle$ are attributed to the shear rate of the spanwise mean flow, because $\partial\langle w \rangle/\partial y$ contributes directly to the production rate of both the shear stresses according to the analysis of the transport equation of shear stresses.

4.2. Thermal statistics

Further, the effects of rotation on turbulent heat transfer are discussed. Fig. 5a shows the profiles of the mean temperature, where $\langle T^+ \rangle$ represents $\langle T^+ \rangle = [\langle T \rangle - T_L]/T_\tau$ with the friction temperature $T_\tau = (\kappa/u_\tau)(|\mathrm{d}\langle T \rangle/\mathrm{d}y|_{y=0})$. Similar to the mean velocity distributions in Fig. 2 there exists a buffer layer followed by a logarithmic region in the mean temperature profile; $\langle T^+ \rangle$ behaves as

$$\langle T^+ \rangle = (1/K_T)\ln y^+ + B_T \tag{5}$$

where K_T and B_T represent the von Kárman constant and the additive constant in the log law of the mean temperature profile. As shown in Fig. 5b, it is confirmed that K_T and B_T depend on N_τ. For the non-rotating flow, i.e., $N_\tau = 0$, Kader and Yaglom [37] found $1/K_T = 2.12$

approximately, which is consistent with our predicted data in Fig. 5b, while Kader [38] gave an empirical expression for the function B_T that describes the experimental results in the logarithmic region of the fully turbulent boundary layer. Based on the temperature profiles in Fig. 5a, both $1/K_T$ and B_T can be obtained in Fig. 5b, where $1/K_T$ increases and B_T decreases with the increase of N_τ.

Fig. 5c shows the profiles of the temperature fluctuation, normalized by the friction temperature. With increasing N_τ, the peak value of temperature fluctuation near the wall increases and their positions shift away the wall. Noted that, when the distance from the wall goes to zero, the temperature fluctuation approaches to zero with a linear slope of y^+; this behavior is almost independent of N_τ.

The Nusselt number is an important parameter relevant to the heat transfer and is defined as

$$Nu = \frac{q_w h}{k\Delta T} \tag{6}$$

where q_w represents the averaged heat flux at the wall, and k is the thermal conductivity. From the mean temperature profiles in Fig. 5a, the Nusselt number is calculated and shown in Fig. 6. It is observed that a linear relationship between Nu and N_τ appears approximately for the range of N_τ considered here. As discussed above, turbulence is suppressed globally with the increase of N_τ; thus it is reasonably predicted that Nu decreases in Fig. 6.

To reveal the characteristics of turbulent heat transfer, Fig. 7 shows the profiles of the turbulent heat fluxes in the streamwise, wall-normal and spanwise directions, respectively, where the temperature fluctuation is normalized by the friction temperature. As N_τ increases, the streamwise and wall-normal turbulent heat fluxes, i.e., $\langle T'^+u'\rangle$ and $-\langle T'^+v'\rangle$, in the near-wall region, are reduced. It is noted that, the spanwise turbulent heat flux, i.e., $-\langle T'^+w'\rangle$, is enhanced apparently when N_τ varies from 0.02 to 0.06, and suppressed when N_τ from 0.06 to 0.1. Since the turbulent heat fluxes are closely related to the velocity fluctuations, the characteristics of turbulent heat

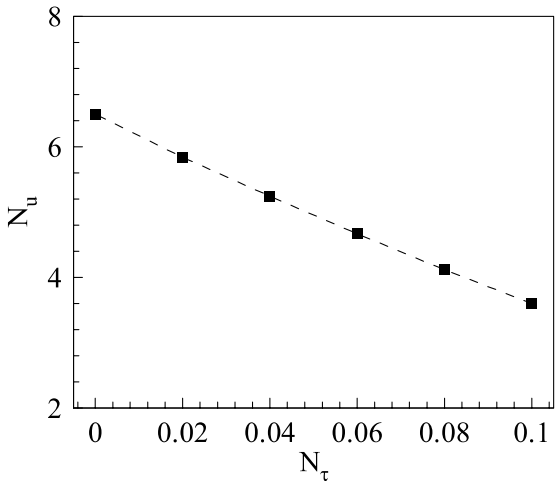

Fig. 6. Profile of the Nusselt number.

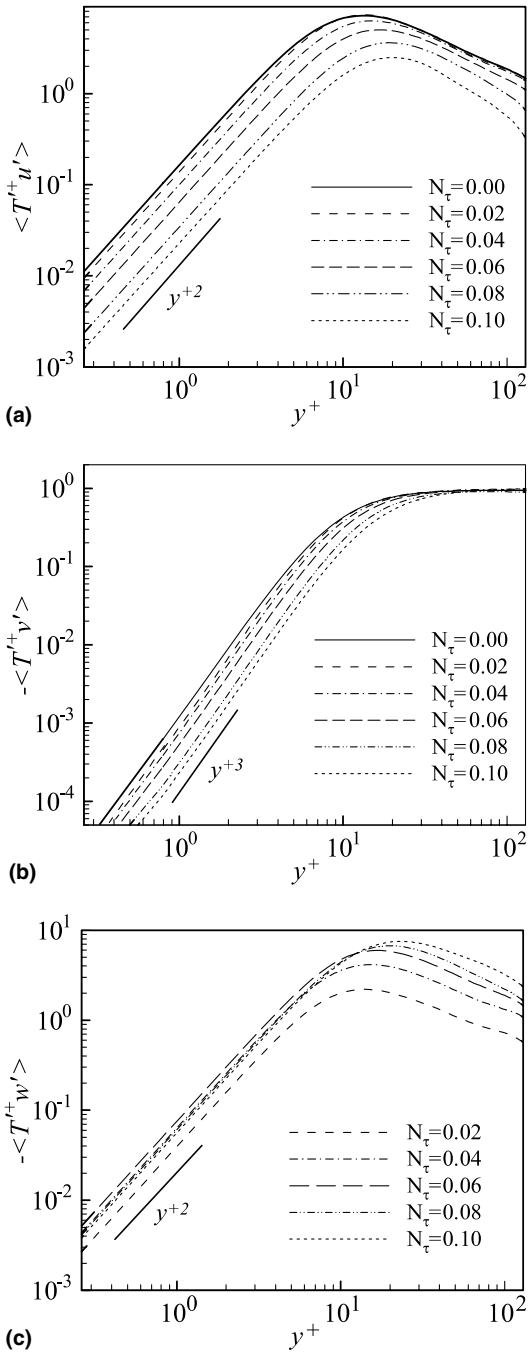

Fig. 7. Distributions of the turbulent heat fluxes in the streamwise (a), wall-normal (b), and spanwise (c) direction.

fluxes versus N_τ are well consistent with the turbulence intensities in Fig. 3.

Furthermore, considering the velocity and temperature boundary conditions, the turbulent heat fluxes $\langle T'^+u'\rangle$, $\langle T'^+v'\rangle$ and $\langle T'^+w'\rangle$ can be expanded into power series of y^+ in the vicinity of the wall,

$$\langle T'^+u'\rangle = a_1 y^{+^2} + a_2 y^{+^3} + \cdots \tag{7a}$$

$$\langle T'^+v'\rangle = b_1 y^{+^3} + b_2 y^{+^4} + \cdots \tag{7b}$$

$$\langle T'^+w'\rangle = c_1 y^{+^2} + c_2 y^{+^3} + \cdots \tag{7c}$$

Then, the curves of the square and cubic laws with y^+ are plotted in Fig. 7 with logarithmic scales to exhibit the first terms in (7). The turbulent heat fluxes agree well with the leading terms in (7) in the near-wall region.

4.3. Thermal budgets

To explore the effects of system rotation on the turbulent heat transfer, we analyze the budget terms in the transport equations of turbulent heat fluxes $\langle T'u_i'\rangle$ shown in Appendix A. Due to the inhomogeneity introduced by the wall, the terms in the budgets have a strong dependence on the distance from the wall and the primary balance involves different terms at different heights.

The budget terms of the streamwise turbulent heat flux $\langle T'u'\rangle$ are shown in Fig. 8a for $N_\tau = 0.06$. In the thermal diffusive sublayer $y^+ < 3$, the budget is balanced mainly between MV_1 and DS_1. In the region around $y^+ = 15$, the terms of $\langle T'u'\rangle$, i.e., PV_1, PT_1, TD_1 DS_1 and MV_1 terms, are mainly contributed to the budget balance and other terms are relatively small. Both PV_1 and PT_1 act as source terms to generate $\langle T'u'\rangle$ over the channel, and MV_1 changes its sign from positive to negative at $y^+ = 6$ approximately. In the core region, all the terms become small. In the rotating case, the non-zero Coriolis force budget term CO_1 arises, however, is negligibly small in comparison with the other terms. To exhibit the effects of rotation on the budget terms in $\langle T'u'\rangle$, the profiles of some typical terms, i.e., PT_1, DS_1 and CO_1, are shown in Fig. 8b–d. With the increase of N_τ, the magnitudes of PT_1 and DS_1 decrease monotonically. By examining the other terms (not shown here), similar tendencies are also found. The CO_1 in Fig. 8d increases versus N_τ and is relatively small.

The budget terms in the transport equation of wall-normal turbulent heat flux, i.e., $\langle T'v'\rangle$, are shown in Fig. 9a for $N_\tau = 0.06$. Note that both PV_2 and CO_2 in Eq. (A1) vanish. In the near-wall region $y^+ < 3$, all the terms are relatively small. In the region around $y^+ = 20$, the budget is balanced mainly between PT_2 and TP_2, and the other terms are relatively small. In Fig. 9b–d, three typical terms, i.e., PT_2, TP_2 and DS_2, are shown. The magnitudes of these terms decrease when the rotation rate increases.

In the wall-normal rotating channel flow, the spanwise mean velocity shown in Fig. 2b is generated and the spanwise turbulent heat flux shown in Fig. 6c occurs. To reveal the mechanism related to the spanwise turbulent heat flux,

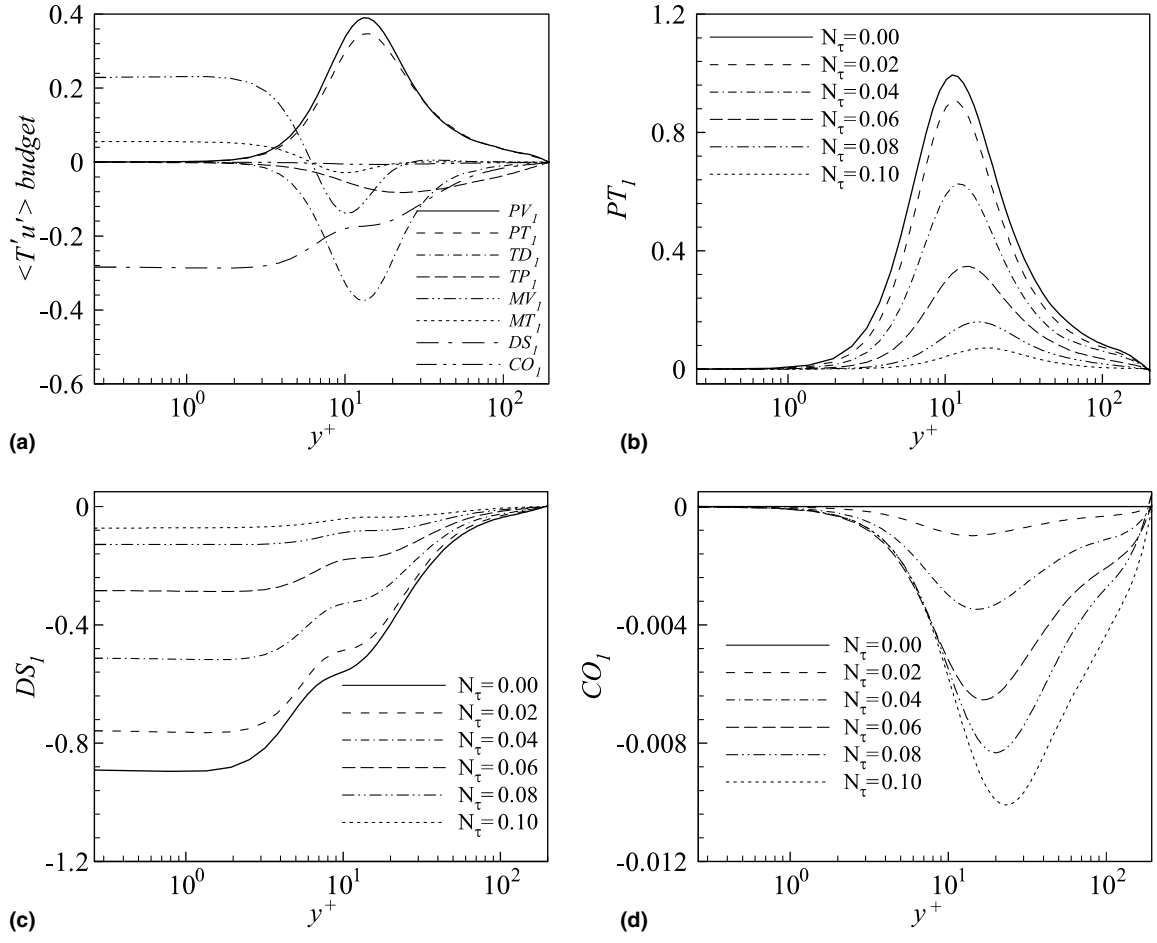

Fig. 8. Distributions of the budget terms in the transport equation of $\langle T'u'\rangle$: (a) budget terms at $N_\tau = 0.06$, (b) PT_1, (c) DS_1, and (d) CO_1.

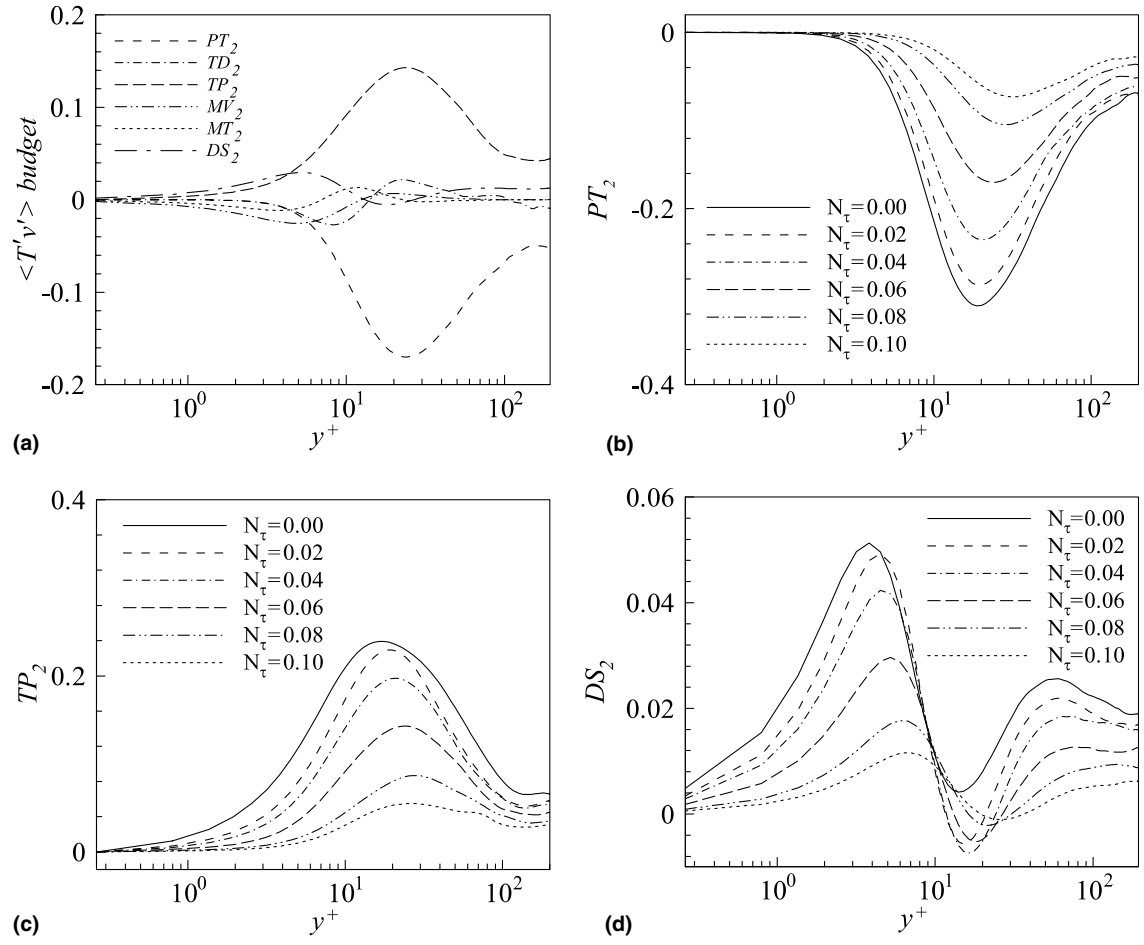

Fig. 9. Distributions of the budget terms in the transport equation of $\langle T'v' \rangle$: (a) budget terms at $N_\tau = 0.06$, (b) PT_2, (c) TP_2, and (d) DS_2.

the budget terms in the transport equation of spanwise turbulent heat flux, i.e., $\langle T'w' \rangle$, are shown in Fig. 10a for $N_\tau = 0.06$. In the thermal diffusive sublayer $y^+ < 3$, DS_3 acts as a dominate term and is balanced mainly with MV_3 and MT_3; this feature is different from the streamwise turbulent heat flux in Fig. 8a. In the region around $y^+ = 15$, all the budget terms, except for CO_3 with negligibly small value, play as a major contribution to the budget balance. In the core region, all the budget terms get small. To exhibit the effects of rotation on the budget terms in $\langle T'w' \rangle$, the profiles of three typical terms, i.e., PT_3, DS_3 and CO_3, are shown in Fig. 10b–d. Similar to the spanwise mean velocity in Fig. 2b and turbulent heat flux in Fig. 6c, the magnitudes of these terms in Fig. 10b–d increase when N_τ varies from 0.02 to 0.06 approximately and decrease when N_τ from 0.06 to 0.1.

Note that, referred to Eq. (A1), the budgets of the streamwise and spanwise turbulent heat fluxes are coupled with each other by the Coriolis force budget terms, which are represented as $N_\tau \langle T'w' \rangle$ and $-N_\tau \langle T'u' \rangle$, respectively. Although the Coriolis force budget terms are relatively small, the Coriolis force actually plays a significant role on turbulence statistics, as shown in Figs. 2–4, which is responsible for thermal statistics.

4.4. Near-wall structures

Structures of the velocity and temperature fluctuations are of great help in exhibiting the influence of the rotation effect on turbulence coherent structures in the near-wall region. Fig. 11 shows the contours of the instantaneous velocity and temperature fluctuations in a plane parallel to the wall at $y^+ = 2.5$. As shown in Fig. 11a, dense elongated streaky structures in the contour plots of the streamwise velocity fluctuation (u') appear at $N_\tau = 0$. With the increase of N_τ, the streamwise velocity fluctuations are significantly suppressed and absent streaky structures occur, in particular for $N_\tau = 0.1$ with a nearly quiescent flow. In Fig. 11b, dense streaky structures of the spanwise velocity fluctuation (w') are observed when N_τ increases to 0.06 approximately, then absent streaky structures are exhibited as N_τ increases further. The features of the streaky structures of the velocity fluctuations agree with the turbulence intensities in Fig. 3a and c. The corresponding instantaneous temperature fluctuation (T') fields are shown in Fig. 11c. One can identify the local spots in accordance with the high- and low-temperature regions alternately. The temperature streaky structures are consistent with those of the velocity fluctuations. These visualizations

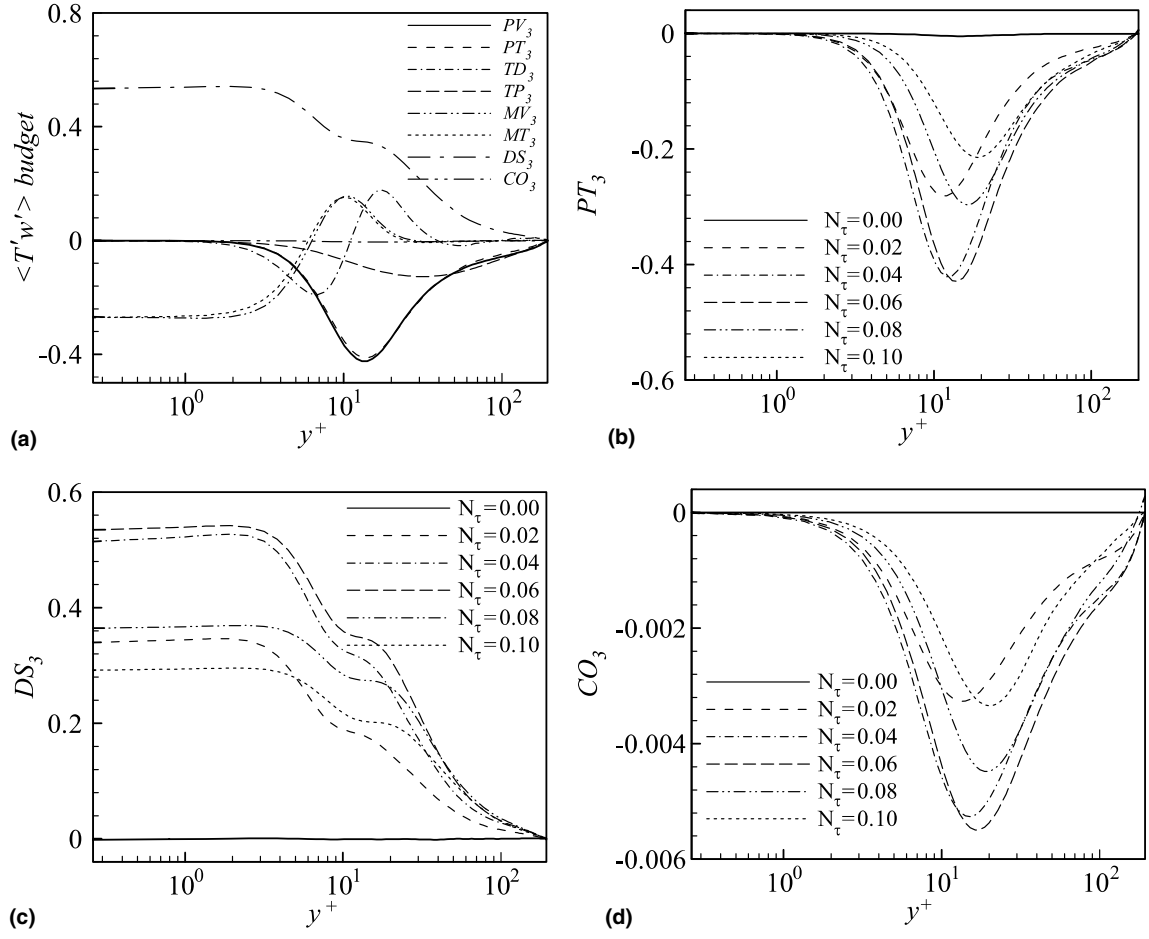

Fig. 10. Distributions of the budget terms in the transport equation of $\langle T'w' \rangle$: (a) budget terms at $N_\tau = 0.06$, (b) PT_3, (c) DS_3, and (d) CO_3.

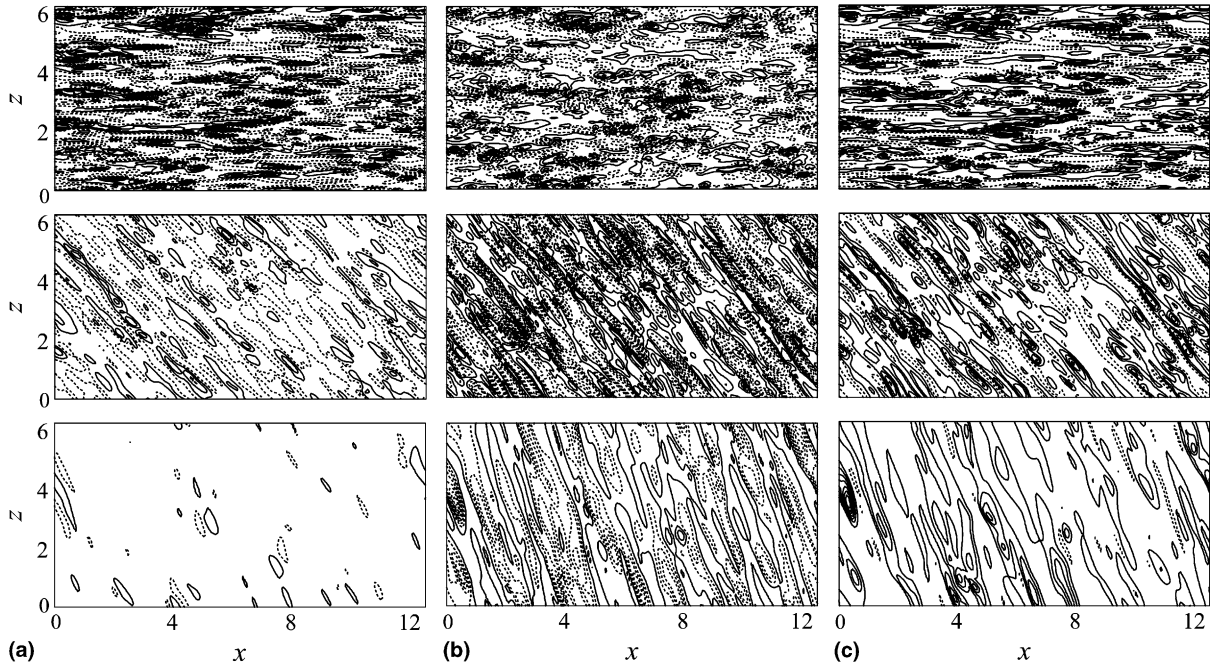

Fig. 11. Contours of the instantaneous velocity and temperature fluctuations in a plane parallel to the wall at $y^+ = 2.5$: (a) u', (b) w', (c) T' with $N_\tau = 0$, 0.06 and 0.1 from the upper panel to the bottom one. Here, solid lines represent positive values and dashed lines negative values. Increments of u', w' and T' are 0.7, 0.3 and 0.02, respectively.

imply that the turbulent mixing of temperature is controlled by turbulence dynamics in the near-wall region.

Due to the rotation effect, the inclined directions of the near-wall structures for the velocity and temperature fluctuations are exhibited obviously. Meanwhile, the contours of the velocity and temperature fluctuations demonstrate the alteration of the streamwise and spanwise separations between the streaky structures in comparison to the non-rotating case. In pure shear channel flow, the streaky structures are exactly aligned with the streamwise direction, arranged along the spanwise direction. This fact accounts for the distributions of the two-point correlations of the

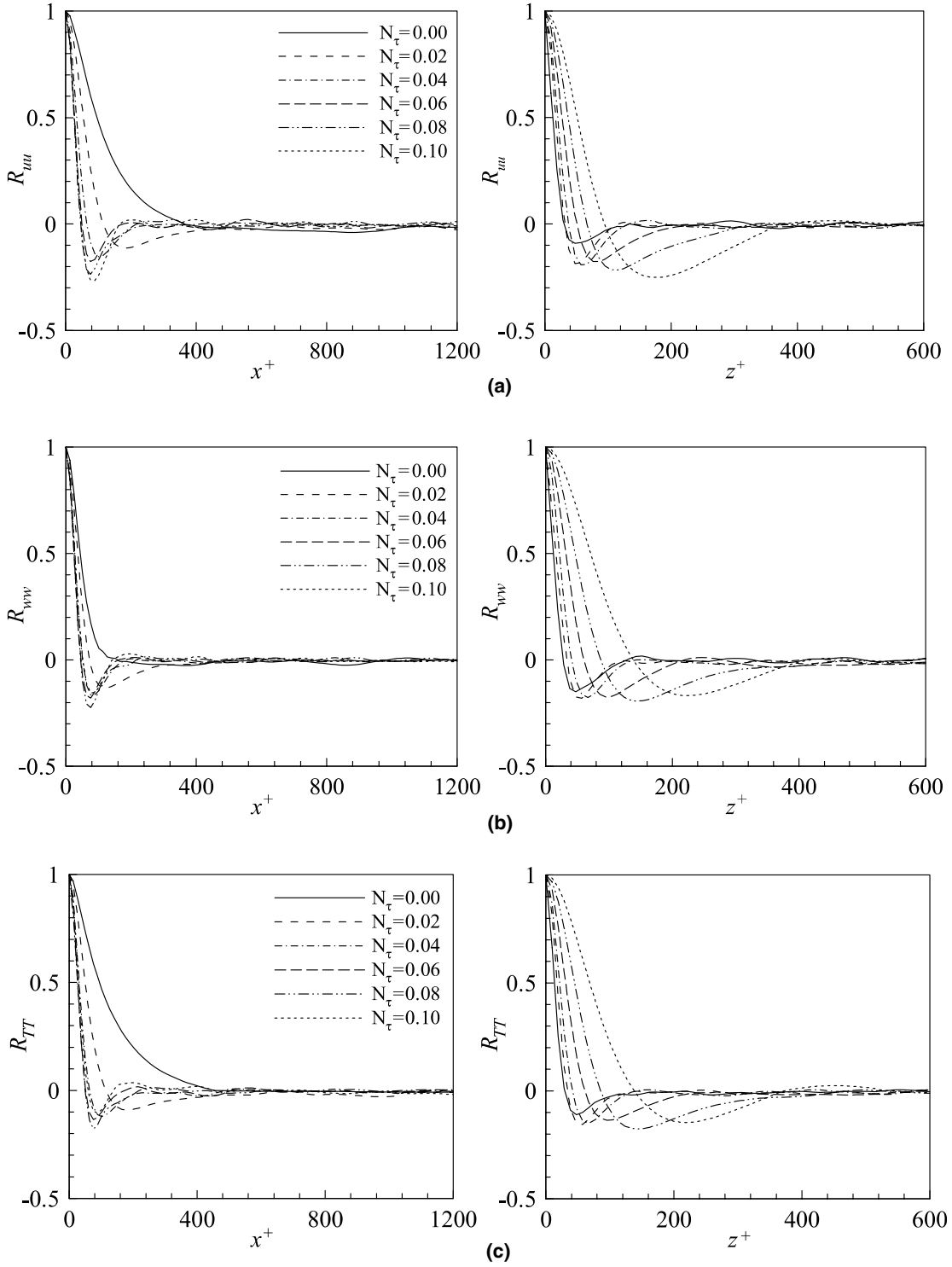

Fig. 12. Two-point correlations of the velocity and temperature fluctuations at $y^+ = 2.5$: (a) R_{uu}, (b) R_{ww}, and (c) R_{TT} in the streamwise (left column) and spanwise (right column) direction.

Table 1
Mean spacing between the wall structures and the inclined angles of the streaky structures at $y^+ = 2.5$

N_τ		0.00	0.02	0.04	0.06	0.08	0.10
R_{uu}	λ_x^+	–	179.7	101.5	76.2	76.6	88.7
	λ_z^+	49.0	54.5	63.1	86.3	115.8	175.8
	λ^+	98.0	104.3	107.2	114.2	127.8	158.4
	θ_λ^u (deg)	0	16.9	31.9	48.5	56.5	63.2
R_{ww}	λ_x^+	–	118.0	83.2	75.4	76.2	82.1
	λ_z^+	47.1	53.3	66.7	95.4	143.6	219.1
	λ^+	94.2	99.1	104.1	118.3	134.6	153.8
	θ_λ^w (deg)	0	24.3	38.7	51.7	62.1	69.5
R_{TT}	λ_x^+	–	179.0	101.4	75.9	76.6	89.0
	λ_z^+	48.5	55.5	65.0	95.8	142.6	218.8
	λ^+	97.0	106.0	109.4	119.0	135.0	164.9
	θ_λ^T (deg)	0	17.2	32.7	51.6	61.8	67.9
$\langle u \rangle$ $\langle w \rangle$	θ_f (deg)	0	17.2	32.3	46.0	54.9	61.6

velocity and temperature fluctuations, i.e., R_{uu}, R_{ww} and R_{TT} gradually falling off to zero along the streamwise direction but exhibiting a distinct minimum along the spanwise direction, as shown in Fig. 12 for $N_\tau = 0$ at $y^+ = 2.5$. In the rotating cases, the streaky structures are nearly aligned with the absolute mean flow, which results in the streamwise separation between the wall streaks, as shown in Fig. 11. Consequently, distinct minimums of the distributions of R_{uu}, R_{ww} and R_{TT} occur not only along the spanwise direction but also along the streamwise direction. As listed in Table 1, the mean separations in the streamwise and spanwise directions are given for different rotation numbers. It is found that the spanwise separations λ_z^+, at which the minimums of R_{uu}, R_{ww} and R_{TT} along in the spanwise direction occur, increases monotonically with the increase of N_τ, indicating the subsequent increase of the spanwise spacing between the streak structures. The streamwise separations λ_x^+, at which the minimums of R_{uu}, R_{ww} and R_{TT} along in the streamwise direction appear, depend on N_τ; they decrease when N_τ varies from 0.02 to 0.06 and increase when N_τ from 0.06 to 0.1. The behaviors of λ_z^+ and λ_x^+ are closely related to the turbulence intensities and are reasonably consistent with results shown in Fig. 3a and c.

The mean spacing between the streaky structures is usually defined as twice the spanwise separation corresponding to minimum R_{uu} in the non-rotating channel flow [17]. This definition also provides an estimate of the mean spacing between the streaky structures in the wall-normal rotating cases. Thus, the mean spacing λ^+ can be obtained by

$$\lambda^+ = 2\lambda_z^+\lambda_x^+ / \sqrt{\lambda_z^{+2} + \lambda_x^{+2}} \tag{8}$$

As listed in Table 1, it is reasonably predicted that the mean spacing λ^+ increases when N_τ increases. Further, the mean inclined angle of the streaky structures with respect to the streamwise direction can be evaluated by

$$\theta_\lambda = \tan^{-1}(\lambda_z^+ / \lambda_x^+) \tag{9}$$

To clearly exhibit the angles, as shown in Table 1, θ_λ^u, θ_λ^w and θ_λ^T represent the angles of the streaky structures based on u', w' and T', respectively. The mean inclined angles increase with N_τ. This behavior is consistent with the profiles of the shear stresses in Fig. 4. As shown in Fig. 3, the spanwise velocity fluctuation w'_{rms} in Fig. 3c becomes stronger when N_τ varies from 0.06 to 0.1, in comparison to the streamwise velocity fluctuation u'_{rms} in Fig. 3a. Since the thermal characteristics are controlled by the turbulence dynamics in the near-wall region, it is thus noted that the values of θ_λ^T are more close to those of θ_λ^u for $N_\tau = 0.02$ and 0.04, and to those of θ_λ^w for $N_\tau = 0.06$, 0.08 and 0.1. Further, the angle (θ_f) based on the mean streamwise and spanwise velocity components at the same (x, z) plane is also calculated and given in Table 1; it is found that the streaky structures are nearly in alignment with the absolute mean flow.

5. Concluding remarks

Fully developed wall-normal rotating turbulent channel flows with heat transfer are investigated numerically for $N_\tau = 0$–0.1, $Re_\tau = 194$ and $Pr = 1$. Two typical rotation regimes are reasonably identified for the parameters considered here. One is weak rotation regime with N_τ from 0 to 0.06, and the other is strong rotation regime with N_τ from 0.06 to 0.1. The streamwise mean velocity $\langle u \rangle$ decreases monotonically with the increase of N_τ, indicating the reduction of wall shear rate related to the streamwise mean flow. Correspondingly, the spanwise mean velocity $\langle w \rangle$ increases when N_τ varies from 0 to 0.06 and decreases when N_τ from 0.06 to 0.1. When $0 < N_\tau < 0.06$, the statistical quantities correlated with the spanwise velocity fluctuation, e.g., the spanwise turbulence intensity w'_{rms}, the shear stresses $\langle v'w' \rangle$ and $\langle u'w' \rangle$, the spanwise turbulent heat transfer $\langle T'^{+}w' \rangle$, are enhanced since the shear rate of spanwise mean flow induced by the Coriolis force increases. However, the other statistical quantities are suppressed. When $N_\tau > 0.06$, all

the statistical quantities are suppressed significantly because the effects of rotation play as dominate role on the rotating flow. Since turbulence is suppressed as the rotation rate increases; it is reasonably predicted that Nu decreases. Based on the analysis of the budget terms in the transport equations of turbulent heat fluxes, although the budget terms associated with the Coriolis force are relatively small, it actually plays a significant role on turbulence statistics, which is responsible for the characteristics of turbulent heat transfer. The near-wall streaky structures of the velocity and temperature fluctuations, redirected by the Coriolis force effect, are proved to be in alignment with the absolute mean flow in the rotating cases. The mean spacing and mean inclined angle of the streaky structures increase obviously with increasing the rotation rate.

Acknowledgements

This work was supported by the National Natural Science Foundation of China (Nos. 90405007, 10302028, 10125210), the China NKBRSF Project (No. 2001CB409600), Specialized Research Fund for the Doctoral Program of Higher Education (No. 20020358013), and the Hundred Talents Programme of the Chinese Academy of Sciences.

Appendix A. Equations for turbulent heat fluxes

The transport equation for the turbulent heat fluxes $\langle T'u_i'\rangle$ in the wall-normal rotating channel flow can be written as

$$\frac{\partial\langle T'u_i'\rangle}{\partial t}+\langle u_j\rangle\frac{\partial\langle T'u_i'\rangle}{\partial x_j}=\mathrm{PV}_i+\mathrm{PT}_i+\mathrm{TP}_i+\mathrm{TD}_i+\mathrm{MV}_i+\mathrm{MT}_i+\mathrm{DS}_i+\mathrm{CO}_i \quad \text{(A1)}$$

The terms on the right-hand side are expressed as

$\mathrm{PV}_i=-\langle u_j'T'\rangle\partial\langle u_i\rangle/\partial x_j$ production rate by mean velocity gradient

$\mathrm{PT}_i=-\langle u_i'u_j'\rangle\partial\langle T\rangle/\partial x_j$ production rate by mean temperature gradient

$\mathrm{TP}_i=-\langle T'(\partial p'/\partial x_i)\rangle$ temperature–pressure gradient correlation

$\mathrm{TD}_i=-\partial\langle u_i'u_j'T'\rangle/\partial x_j$ turbulent diffusion

$\mathrm{MV}_i=1/Re_\tau\langle\partial/\partial x_j[T'(\partial u_i'/\partial x_j)]\rangle$ molecular diffusion relevant to velocity fluctuation

$\mathrm{MT}_i=1/(Re_\tau Pr)\langle\partial/\partial x_j[u_i'(\partial T'/\partial x_j)]\rangle$ molecular diffusion relevant to temperature fluctuation

$\mathrm{DS}_i=-[1/Re_\tau+1/(Re_\tau Pr)]\langle(\partial u_i'/\partial x_j)(\partial T'/\partial x_j)\rangle$ dissipation rate

$\mathrm{CO}_i=-\varepsilon_{ijk}N_\tau(\Omega_j/|\Omega|)\langle u_k'T'\rangle$ Coriolis force budget

References

[1] H.B. Wu, N. Kasagi, Effects of arbitrary directional system rotation on turbulent channel flow, Phys. Fluids 16 (2004) 979–990.
[2] J.P. Johnston, R.M. Halleen, D.K. Leziius, Effects of spanwise rotation on the structure of two-dimensional fully developed turbulent channel flow, J. Fluid Mech. 56 (1972) 533–557.
[3] R. Kristoffersen, H.I. Andersson, Direct simulations of low-Reynolds number turbulent flow in a rotating channel, J. Fluid Mech. 235 (1993) 163–197.
[4] U. Piomelli, J. Liu, Large-eddy simulation of rotating channel flows using a localized dynamic model, Phys. Fluids 7 (1995) 839–848.
[5] K. Nakabayashi, O. Kitoh, Low Reynolds number fully developed turbulent channel flow with system rotation, J. Fluid Mech. 315 (1996) 1–29.
[6] E. Lamballais, O. Metais, M. Leiseur, Spectral-dynamical model for large-eddy simulations of turbulent rotating channel flow, Theor. Comput. Fluid Dyn. 12 (1998) 149–177.
[7] Y. Nagano, H. Hattori, Direct numerical simulation and modelling of spanwise rotating channel flow with heat transfer, J. Turbulence 4 (2003) 10.
[8] M. Oberlack, W. Cabot, M.M. Rogers, Turbulent channel flow with streamwise rotation: Lie group analysis, DNS, and modeling, in: Proc. First Int. Symp. Turbulence and Shear Flow Phenomena, Santa Barbara, CA, 12–15 September 1999, pp. 85–90.
[9] I. Esau, The Coriolis effect on coherent structures in planetary boundary layers, J. Turbulence 4 (2003) 17.
[10] C.G. Speziale, B.A. Younis, R. Rubinstein, Y. Zhou, On consistency condition for rotating turbulent flows, Phys. Fluids 22 (1998) 2108–2110.
[11] Y. Nagano, H. Hattori, An improved turbulence model for rotating shear flows, J. Turbulence 3 (2002) 6.
[12] H. Kawamura, K. Ohsaka, H. Abe, K. Yamamoto, DNS of turbulent heat transfer in channel flow with low to medium–high Prandtl number fluid, Int. J. Heat Fluid Flow 19 (1998) 482–491.
[13] H. Kawamura, H. Abe, Y. Matsuo, DNS of turbulent heat transfer in channel flow with respect to Reynolds and Prandtl number effects, Int. J. Heat Fluid Flow 20 (1999) 196–207.
[14] R. Verzicco, P. Orlandi, A finite difference scheme for direction simulation in cylindrical coordinates, J. Comput. Phys. 123 (1996) 402–414.
[15] J. Kim, P. Moin, Application of a fractional-step method to incompressible Navier–Stokes equations, J. Comput. Phys. 59 (1985) 308–323.
[16] M.M. Rai, P. Moin, Direct simulations of turbulent flow using finite-difference schemes, J. Comput. Phys. 96 (1991) 15–53.
[17] J. Kim, P. Moin, R. Moser, Turbulence statistics in fully developed channel flow at low Reynolds number, J. Fluid Mech. 177 (1987) 133–166.
[18] P. Orlandi, Helicity fluctuations and turbulent energy production in rotating and non-rotating pipes, Phys. Fluids 9 (1997) 2045–2056.
[19] P. Orlandi, D. Ebstein, Turbulent budgets in rotating pipes by DNS, Int. J. Heat Fluid Flow 21 (2000) 499–505.
[20] P. Orlandi, M. Fatica, Direct simulations of turbulent low in a pipe rotating about its axis, J. Fluid Mech. 343 (1997) 43–72.
[21] Y.K. Pan, T. Tanaka, Y. Tsuji, Direct numerical simulation of particle-laden rotating turbulent channel flow, Phys. Fluids 13 (2001) 2320–2337.
[22] S.Y. Chung, G.H. Rhee, H.J. Sung, Direct numerical simulation of turbulent concentric annular pipe flow Part 1: flow field, Int. J. Heat Fluid flow 23 (2002) 426–440.
[23] G. Vittor, R. Verzicco, Direct simulation of transition in an oscillatory boundary layer, J. Fluid Mech. 371 (1998) 207–232.
[24] M. Quadrio, S. Sibilla, Numerical simulation of turbulent flow in a pipe oscillating around its axis, J. Fluid Mech. 424 (2000) 217–241.
[25] S. Grossmann, D. Lohse, On geometry effects in Rayleigh–Bénard convection, J. Fluid Mech. 486 (2003) 105–114.
[26] N.S. Liu, X.Y. Lu, Large eddy simulation of turbulent concentric annular channel flows, Int. J. Numer. Meth. Fluids 45 (2004) 1317–1338.

[27] Y.H. Dong, X.Y. Lu, Large eddy simulation of a thermally stratified turbulent channel flow with temperature oscillation on the wall, Int. J. Heat Mass Transfer 47 (2004) 2109–2122.
[28] L. Wang, X.Y. Lu, An investigation of turbulent oscillatory heat transfer in channel flows by large eddy simulation, Int. J. Heat Mass Transfer 47 (2004) 2161–2172.
[29] L. Wang, Y.H. Dong, X.Y. Lu, An investigation of turbulent open channel flow with heat transfer by large eddy simulation, Comput. Fluids 34 (2005) 23–47.
[30] X.Y. Lu, S.W. Wang, H.G. Sung, S.Y. Hsieh, V. Yang, Large eddy simulations of turbulent swirling flows injected into a dump chamber, J. Fluid Mech. 527 (2005) 171–195.
[31] L. Wang, X.Y. Lu, Large eddy simulation of stably stratified turbulent open channel flows with low- to high-Prandtl number, Int. J. Heat Mass Transfer 48 (2005) 1883–1897.
[32] N.S. Liu, X.Y. Lu, L.X. Zhuang, Rotation effect on near-wall turbulence statistics and flow structures, Sci. China G 48 (2005) 211–227.
[33] Y.H. Dong, X.Y. Lu, Direct numerical simulation of stably and unstably stratified open channel flows, Acta Mech. 177 (2005) 115–136.
[34] D.J. Tritton, Stabilization and destabilization of turbulent shear flow in a rotating fluid, J. Fluid Mech. 241 (1992) 503–523.
[35] P. Moin, J. Kim, Numerical investigation of turbulent channel flow, J. Fluid Mech. 118 (1982) 341–377.
[36] H. Tennekes, J.L. Lumley, A First Course in Turbulence, MIT Press, Cambridge, MA, 1972, pp. 95–97.
[37] B.A. Kader, A.M. Yaglom, Heat and mass transfer laws for fully turbulent wall flows, Int. J. Heat Mass Transfer 15 (1972) 2329–2342.
[38] B.A. Kader, Temperature and concentration profiles in fully turbulent boundary layers, Int. J. Heat Mass Transfer 24 (1981) 1541–1545.